

Original Article Published in Journal of Biomechanics
Full reference: Van der Merwe H, Reddy BD, Zilla P, Bezuidenhout D,
Franz T. A computational study of knitted Nitinol meshes for their
prospective use as external vein reinforcement. J Biomech, 2008,
41(6), 1302-9

A Computational Study of Knitted Nitinol Meshes for Their Prospective Use as External Vein Reinforcement

Helena van der Merwe¹, B. Daya Reddy², Peter Zilla¹, Deon Bezuidenhout¹, Thomas Franz¹

¹Cardiovascular Research Unit

²Centre for Research in Computational and Applied Mechanics

University of Cape Town, Cape Town, South Africa

Keywords: External reinforcement; Vein grafts, Nitinol, Finite element modelling, Compliance

Send correspondence to:

Dr Thomas Franz

Cardiovascular Research Unit

University of Cape Town / Faculty of Health Sciences

7925 Observatory

Cape Town

South Africa

Tel: +27-21-406 6418

Fax: +27-21-448 5935

e-mail: thomas.franz@uct.ac.za

ABSTRACT

External reinforcement has been suggested for autologous vein grafts to address the mismatch of mechanical properties and fluid dynamics of graft and host vessel, a main factor for graft failure. A finite element tool was developed to investigate the mechanical behaviour, in particular radial compliance, of knitted Nitinol meshes (internal diameter: 3.34 mm) with two different knit designs (even versus uneven circumferential loops) and three different wire thicknesses (0.05, 0.0635 and 0.075 mm) under physiological conditions. The Nitinol material parameters were obtained from experimental testing. The compliance predicted for the 80-120 mmHg physiological blood pressure range was 2.5, 0.9 and 0.6 %/100mmHg for the even loop design and 1.2, 0.5 and 0.5 %/100mmHg for the uneven loop design, for wire thicknesses of 0.05, 0.0635 and 0.075 mm. The highest stress, at 120 mmHg, was found in the even loop mesh with the thinnest wire to be 268 MPa, remaining 44.5 % below the stress initiating stress-induced phase transformation. The maximum stress decreased to 132 and 91 MPa with increasing wire thickness of the same loop design. The uneven loop design exhibited maximum stress levels of 65.3, 63.6 and 87.9 % of the even loop values at 0.05, 0.0635 and 0.075 mm wire thickness. The maximum strain of 0.7 %, at 120 mmHg, remained un-critical considering a typical high-cycle recoverable strain of 2 %. It was demonstrated that the numerical approach developed is feasible of effectively evaluating design variations of knitted Nitinol meshes towards vein graft behaviour equivalent to arterial mechanics.

1. INTRODUCTION

Blood vessels have particular and site-specific mechanical properties which help fulfilling their role within the circulatory system. Native arteries change the diameter cyclically in response to blood pressure variation during a cardiac cycle. This behaviour derives in part from their layered structure with layer-wise distinct mechanical properties (Keener and Sneyd, 1998; Nichols and O'Rourke, 1998; Shadwick, 1998, 1999).

Various treatments for arterial diseases such as angioplasty, intravascular stenting, and vascular grafting are available (O'Rourke, 1995). The work presented here focuses on an aspect of vascular grafting using autologous veins as bypass conduits.

The difference in mechanical properties between grafts and host arteries is a complicating factor for vascular bypass surgery and can cause patho-physiological problems after implantation (Surovtsova, 2005; Salacinski et al., 2001; Mehta et al., 1997, 1998; Lemson et al., 2000; Sarkar et al., 2006; Seifalian et al., 1999; Gupta and Kasyanov, 1997; Lei et al., 1997). A multi-component structure has been proposed for vascular grafts similar to arteries in order to more closely approximate arterial mechanical properties.

One such option, investigated here, is a recoil-compliant external Nitinol mesh for vein grafts. The objectives of this study were: a) to develop a numerical tool, based on the Finite Element (FE) method, to simulate the mechanical behaviour and assess the mechanical and structural properties, such as radial compliance, of knitted Nitinol structures, and b) to demonstrate the feasibility of the numerical tool for the evaluation of effects of design variations on the mechanical and structural properties of the Nitinol structures, consequently aiming at the identification of optimal structural designs which provide desired mechanical characteristics.

2. MATERIALS AND METHODS

2.1 Nitinol Material Model

The Nitinol material was modelled as a predefined user material in ABAQUS CAE 6.4-5 (Abaqus Inc., Providence, RI, USA), a proprietary FE software package. Most values required for the ABAQUS shape memory user material (SM-UMAT) were determined from experimental tensile tests of wire samples (length: 100 mm, diameter: 0.05, 0.064, and 0.075 mm). Tests were conducted on an INSTRON 5544 tensile testing machine with a 500 N load cell. Samples remained submerged in distilled water throughout the test to provide physiological temperature of 37°C. The experimental procedure comprised 99 cycles from 1 to 4.5 % strain (first cycle

starting at 0 % strain), followed by two cycles from 1 to 8 % strain and a final loading from 1 to 20 % strain. The cycling was conducted at a cross-head speed of 38 mm/min. Effects of the test medium, distilled water compared to saline or serum, on the experimental results were not expected due to the limited test duration of ca. 20 mins. Material parameters marked with source “Test” in Table 1 were determined as grand means of all samples tested. For the remaining parameters, which could not be determined by tensile testing, values were obtained from Medtronic Vascular Galway.

The Nitinol material parameters used in the ABAQUS SM-UMAT are summarised in Table 1. The material model was verified by comparing the results of a numerical tensile test to those of experimental tensile tests.

2.2 FE Models of Nitinol Meshes

The tubular knitted Nitinol wire meshes featured an internal diameter of 3.34 mm. The distinguishing design features were: a) uneven and even circumferentially adjacent loop pairs (see Fig. 1) and b) wire thicknesses of 0.05, 0.064 and 0.075 mm. The repeatability of the meshes allowed for only a portion to be analysed. The three-dimensional solid geometry of a single loop was imported into ABAQUS CAE 6.4-5 and partitioned in longitudinal and circumferential wire direction (illustrated in Fig. 2). Three loops were arranged in longitudinal mesh direction to assemble the model geometry. Partial loop sections, added to the longitudinal ends of the assembly, assisted in the definition of boundary conditions.

Tri-linear brick elements were used in all models. The mesh density was refined from 4 elements through the wire thickness in loop regions with low curvature to 6 and 8, respectively, elements through the wire thickness in loop regions with large curvature, i.e areas of expected stress concentrations. The number of elements in the final models varied between 25,000 and 64,000 depending on loop geometry, wire thickness, and partitioning. Boundary conditions, element type and mesh density were verified through comparative analyses with parameter variations. Softened contact definitions defined contact between the expander and the wires, and between wire surfaces at cross-over sections. Tie constraints were used between partition interfaces.

An axis-symmetric radial displacement was applied, linearly over time, to the mesh using a fictitious cylindrical surface (“expander”) which extended circumferentially to a 45°-section and longitudinally over the length of the loop assembly (see Fig. 3). The fictitious surface, a user-defined Fortran code (Compaq Visual Fortran 6.6A, Compaq Computer Corporation, Houston, TX, USA) incorporated into ABAQUS, allowed for the loading without increasing the computational costs.

The primary independent variable for the analysis was the expander radius. The analysis was executed in two steps: 1) Establishing contact between expander and loop assembly and 2) Radial displacement (dilation) of expander and loop assembly.

2.3 Data Capture and Analysis

The maximum principal stress and strain at integration points and the reaction force of the mesh onto the expander were captured at each time increment during the analyses.

Radial, or diametric, compliance of a vascular graft relates a change in graft diameter to the underlying change in luminal pressure. The luminal pressure was, however, not directly available in the analyses; it was not used as input (distension of the Nitinol mesh induced through radial displacement) and not captured as output parameter (fictitious expander surface prevented implicit derivation of pressure). Consequently, the luminal pressure, P_i , had to be derived from the effective reaction force, $F_{\text{eff},i}$, of the mesh onto the expander and the expander surface area at each time increment, i , assuming an even pressure distribution over the non-deformable expander surface:

$$P_i = \frac{F_{\text{eff},i}}{LR_i\sqrt{2-2\cos\theta}}, \quad (1)$$

where R_i is the prescribed expander radius, L is the length of the expander in longitudinal mesh direction, and θ is the angle subtending the expander surface (see Fig. 3). The radial compliance, C_D , was calculated from two pressure-radius pairs (P_i, R_i) for the diastolic-systolic pressure range 80-120 mmHg using Eq. (2):

$$C_D = \frac{R_2 - R_1}{(P_2 - P_1)R_1} \quad (2)$$

3. RESULTS

The primary output variables were the reaction force of the mesh, maximum principal stress and maximum principal strain. The luminal pressure and radial compliance were calculated as described above to relate the numerical results to physiological parameters.

The numerical analyses were conducted with automatically controlled time increments to ensure the fastest possible convergence. Hence, diameter and pressure increments could not be explicitly controlled and numerical results refer to pressure values closest to target pressure values of 80 and 120 mmHg, as specified in Table 2.

Figure 4 illustrates the change in the derived luminal pressure with change in inner mesh diameter. For even and uneven loop design it was observed that the pressure increased more rapidly with mesh dilation as the wire thickness increased. For the even loop mesh with 0.05 mm wire thickness, the pressure increased steadily with increasing mesh diameter from 0 mmHg. All other models displayed a slightly different behaviour; a similar initial pressure change with diameter increase irrespective the wire thickness up to approximately 10 mmHg, above which the difference in wire thickness came into effect. The diameter increase at the transition at approximately 10 mmHg varied between 0.2 and 1.6 % for the different meshes.

The compliance at 80-120 mmHg was 2.51, 0.92 and 0.63 %/100 mmHg for the even loop design and 1.17, 0.52 and 0.51 %/100 mmHg for the uneven loop design, for the wire thicknesses of 0.05, 0.0635 and 0.075 mm (see also Table 2). The compliance decreased with increasing wire thickness irrespective the loop design, exhibiting a more distinct reduction between 0.05 and 0.0635 mm (63.3 % and 55.6 % for even and uneven loop design) than between 0.0635 and 0.075 mm (31.5 % and 1.9 % for even and uneven loop design). The even loop design promoted a higher compliance than the uneven loop design for each wire thickness. The difference became more pronounced with decreasing wire thickness; the compliance increase was 23.5, 76.9 and 114.5 % for the wire thickness of 0.075, 0.0635 and 0.05 mm.

The maximum principal stress and strain at 120 mmHg is summarized in Table 2. For both loop designs, stress and strain reached highest levels for the thinnest wire (0.05 mm) and decreased with increasing wire thickness. Similarly to the change in compliance, the decrease in maximum stress and strain was more pronounced between smallest and medium wire thickness than between medium and largest thickness. For the even loop design, the maximum principal stress decreased by 50.7 % from 268 MPa (0.05 mm wire thickness) to 132 MPa (0.0635 mm wire thickness) and further by 31.1 % to 91 MPa (0.075 mm wire thickness). For the uneven loop design, the maximum principal stress decreased by 52.0 % (175 MPa at 0.05 mm wire thickness to 84 MPa at 0.0635 mm wire) and further by 4.8 % (80 MPa at 0.075 mm wire thickness). The even loop design experienced 53.1, 57.1 and 13.8 % higher maximum principal stress than the uneven loop design for 0.05, 0.0635 and 0.075 mm wire thickness. The maximum principal strains displayed a different variation between even and uneven loop designs of the same wire thickness: -1.4, 4.9 and 21.9 % (0.05, 0.0635, 0.075 mm wire thickness).

The distributions of the maximum principal stress and strain at 120 mmHg are shown in Figs. 5 and 6, respectively, for even and uneven loop geometry of 0.0635 mm wire thickness. The locations of stress and strain concentrations were predicted to coincide centrally in the loop heads and in contact areas of wire crossovers (representative for all wire thicknesses). For the uneven loop geometry, maximum stress concentrations were observed in the head of the narrow loops with lower stress levels in the wider loop.

4. DISCUSSION

This study was concerned with the development of a computational approach which can be used to evaluate the design of knitted Nitinol meshes. The approach incorporates the representation of a non-linear elastic Nitinol material exhibiting stress-induced phase transformation (superelasticity) and thin-wire knit geometries, both of which are non-trivial and computationally expensive. One challenge of this study was, therefore, to limit the numerical complexity yet to provide meaningful evaluation parameters in the framework of vascular grafts. This was successfully achieved by carefully selecting the methods to simulate the expected in-vivo mechanics of the knitted structures. User-defined algorithms were developed for: a) defining auxiliary components of the model not adding to computational expense but allowing for realistic simulation of the mechanics, such as the expander surface used to exert dilation displacement onto the knit structure, and b) creating and processing output data so as to provide cardiovascular relevant evaluation parameters, such as the radial compliance depending on luminal pressure which was, however, not used as input parameter and not available as a standard output parameter for the approach utilised.

A case study investigating six mesh variations (two loop designs and three wire thicknesses) demonstrated the versatility and numerical stability of the FE tool developed. The results suggest that the even loop design combined with the thinnest Nitinol wire offers most potential for providing arterial-like mechanics.

The graphs of pressure-diameter change indicated a decrease in radial compliance as the wire thickness increased (Fig. 4). All meshes with exception of the even loop design with 0.05 mm wire thickness exhibited a piece-wise near-linear pressure-diameter relationship with two distinct regions. It is suggested that the transition from the initial high-compliance region to the low-compliance region, at a pressure of approximately 10 mmHg, was characterised by the engagement of the intersecting wires of longitudinally interconnected loops from non-contact to contact. Prior to loop engagement, the dilation of the mesh seemed to occur without, or with minimal, deformation of the loops resulting in reduced structural stiffness of the mesh. The structural stiffness increased after the loops engaged causing a decrease in compliance. For the mesh with even loops and 0.05 mm wire thickness, the non-linear pressure-diameter curve with absence of the characteristic transition is ascribed to a concurrent engagement of wire and loop bending deformation from zero pressure.

The initial high-compliance phase suggests the influence of longitudinal deployment of the mesh on its radial mechanics: Ensuring the engagement of the linked wires during deployment can prevent this initial phase. The practical relevance of the initial high-compliance dilation has

however to be further evaluated since: 1) this phase is completed at approximately 15 mmHg, i.e. far below physiological pressure, and 2) the initial diameter increase observed was maximum 1.6 %, i.e. approximately 0.05 mm considering the initial internal mesh diameter of 3.34 mm.

The numerically predicted radial compliance of the meshes between 0.51 and 2.51 %/100 mmHg for the physiological pressure range of 80-120 mmHg confirmed the findings of an increase in compliance with decreasing wire thickness. The reduction of the wire thickness of the presented mesh designs is a potential means to further increase the compliance, in particular due to the indication of an exponential increase of compliance with reduction of wire thickness for the even loop design. This needs, however, careful evaluation in the context of stresses and strains exhibited in the meshes.

The highest stress of 268 MPa observed in the even loop mesh with 0.05 mm wire thickness featuring the highest compliance exceeded the maximum stress of 175 MPa in the uneven loop design with the same wire thickness by 153.1 %, whereas maximum strains were similar at 0.70 and 0.71 % in even and uneven loop designs. Both maximum stress and strain values remain below critical values and may allow for Nitinol wires thinner than 0.05 mm to be used to achieve higher radial compliance. The maximum stress level predicted remained 44.5 and 56.1 % below stress associated with the start and end of stress-induced phase transformation to Martensite during loading. Cyclic softening may lead to a decrease of the stress amplitude and consequently a reduction of the safety margin. This phenomenon is however predominantly associated with the stress region of the Martensite transformation (Tolomeo, 2001), which the predicted stresses did not reach. Although fatigue of the Nitinol wires has not been studied here, a typical value for the recoverable strain of Nitinol for loadings beyond 100,000 cycles is reported to be 2 % (NN, 2006). This strain limit offers a potential margin of 185 % increase in the maximum strain at 120 mmHg. For further design optimisation and detailed assessment of critical loads and fatigue, it however needs to be taken into account that peak blood pressure exceeds 120 mmHg resulting in increased loads.

The locations of the stress concentrations coincided with those of the strain concentrations. Concentrations occurred predominantly in areas of high curvature (loop heads) and contact areas of wire cross-overs between adjacent loops. The uneven loop geometry exhibited higher stresses in the narrow loop than in the wide loop. However, maximum stress levels in the even loop geometry exceeded those in the narrow uneven loops despite a smaller loop curvature.

The numerical tool presented has potential for future extension since only a limited representation of the vascular mechanics has been incorporated in its current version. While it offers a valuable means for basic comparative design studies of knitted Nitinol structures, such as radial compliance in the mid-graft region, it is desirable to also evaluate the Nitinol knits in more complex problems. A prominent topic in vascular grafting is the anastomotic mechanics –

an important determinant for graft performance and failure. Investigating the Nitinol structures in the anastomotic environment will require a considerable adaptation of the current numerical tool. This includes the incorporation of: a) vascular soft tissue, both arterial for the host/target vessel and venous for the graft, b) fluid mechanics of the blood flow, and c) fluid-structure interaction between the blood and the vascular graft and host vessel, respectively. Apart from these cardiovascular more complex problems, more in-depth attention must, in future, also be focussed to the fatigue and failure mechanics of the Nitinol structures.

5. CONCLUSIONS

The objective of this study was to establish a computational tool for the analysis of the effect of design variations of knitted Nitinol meshes on their mechanical behaviour and structural integrity with the aim of optimisation towards arterial mechanics. It was successfully demonstrated that the developed numerical approach can be employed to comparatively evaluate different mesh designs and structural variations, and their effects on mechanical performance. The results of this study offer guidance for further design optimisation of these knitted meshes such as even loop design and reduced thickness of the Nitinol wire being potential keys for increased radial compliance. Other design parameters to be investigated may include number of circumferential loops, knit tension, and longitudinal deployment. Advances of the numerical tool may be a more detailed analysis of fatigue, an incorporation of complementing graft components (such as vascular soft tissue), axial load cases, and anastomotic mechanics. The benefits of more comprehensive numerical models need, however, to be assessed against the increased computational expenses. This is in particular important since the non-trivial constitutive model for the shape memory alloy Nitinol will then be combined with a similar complex material model for soft tissue.

Overall, the numerical approach presented can lead to a better understanding of the complex mechanics of knitted Nitinol structures and provide guidelines for further design optimisation towards vascular grafts with near-physiological properties.

ACKNOWLEDGEMENTS

The authors wish to thank Michael F. Wolf and Don Rutledge (Medtronic Inc., Minneapolis, MN, USA), Nasser Rafiee and Nareak Douk (Medtronic Vascular, Danvers, MA, USA), and Brendan Cunniffe (Medtronic Vascular, Galway, Ireland) for their excellent assistance in geometrical modelling, mesh manufacturing, and numerical modelling.

The study was mainly funded through a research collaboration grant by Medtronic Inc. (Minneapolis, MN, USA) to the University of Cape Town and a THRIPP grant of the National Research Foundation (South Africa). Mesh manufacture was directly funded by Medtronic Inc. (Minneapolis, MN, USA) and Medtronic Vascular (Danvers, MA, USA).

REFERENCES

Gupta, B.S., Kasyanov, V.A., 1997. Biomechanics of human common carotid artery and design of novel hybrid textile compliant vascular grafts. *Journal of Biomedical Materials Research* 34, 341-349.

Keener, J., Sneyd, J., 1998. *Mathematical Physiology*. Springer, New York.

Lei, M., Archie, J.P., Kleinstreuer, C., 1997. Computational design of a bypass graft that minimizes wall shear stress gradients in the region of distal anastomosis. *Journal of Vascular Surgery* 25, 637-346.

Lemson, M.S., Tordoir, J.H., Daemen, M.J., Kitslaar, P.J., 2000. Intimal hyperplasia in vascular grafts. *European Journal of Vascular and Endovascular Surgery* 19, 336-350.

Mehta, D., George, S.J., Jeremy, J.Y., Izzat, M.B., Southgate, K.M., Bryan, A.J., Newby, A.C., Angelini, G.D., 1998. External stenting reduces long-term medial and neointimal thickening and platelet derived growth factor expression in a pig model of arteriovenous bypass grafting. *Nature Medicine* 4, 235-239.

Mehta, D., Izzat, M.B., Bryan, A.J., Angelini, G.D., 1997. Towards the prevention of vein graft failure. *International Journal of Cardiology* 62, s55-s63.

Nichols, W.W., O'Rourke, M., 1998. *McDonald's blood flow in arteries. Theoretical, experimental and clinical principles*. Arnold, London.

NN, 2006. Info sheet No. 4: Selected properties of NiTi. (http://www.memory-metalle.de/html/03_knowhow/PDF/MM_04_properties_e.pdf). Memory Metalle GmbH, Weil am Rhein.

O'Rourke, M., 1995. Mechanical principles of arterial disease. *Hypertension* 26, 2-9.

Salacinski, H.J., Goldner, S., Giudiceandrea, A., Hamilton, G., Seifalian, A.M., Edwards, A., Carson, R.J., 2001. The mechanical behaviour of vascular grafts: a review. *Journal of Biomaterials Applications* 15, 241-278.

Sarkar, S., Salacinski, H.J., Hamilton, G., Seifalian, A.M., 2006. The mechanical properties of infrainguinal vascular bypass grafts: Their role in influencing patency. *European Journal of Vascular and Endovascular Surgery* 31, 629-636.

Seifalian, A.M., Giudiceandrea, A., Schmidz-Rixen, T., Hamilton, G., 1999. Noncompliance: The silent acceptance of a villain. In: Zilla, P., Greisler, H.P. (Eds.), *Tissue Engineering of Prosthetic Vascular Grafts*. R.G. Landes Company, Austin, 45-58.

Shadwick, R.E., 1998. Elasticity in arteries. *American Scientist* 86, 535.

Shadwick, R.E., 1999. Mechanical design in arteries. *Journal of Experimental Biology* 202, 3305-3313.

Surovtsova, I., 2005. Effects of compliance mismatch on blood flow in an artery with endovascular prosthesis. *Journal of Biomechanics* 38, 2078-2086.

Tolomeo, D., Davidson, S., Santinoranont, M., 2000. Cyclic properties of superelastic Nitinol: Design implications. In *SMST-2000 Proceedings of the International Conference on Shape Memory and Superelastic Technology*. Pacific Grove.

Tables

Table 1. Parameters required in ABAQUS user material sub-routine for shape memory materials and parameter values used in this study. Data sources: “Test” indicates values which originate from experimental tests conducted by the authors. “MDT” indicates data obtained from research collaborators

Parameter	Symbol	Unit	Value	Source
Austenite Young’s modulus	E_A	MPa	38992	Test
Austenite Poison’s ratio	ν_A	-	0.46	MDT
Martensite Young’s modulus	E_M	MPa	21910	Test
Martensite Poison’s ratio	ν_M	-	0.46	MDT
Transformation strain	ε^L	-	0.042	Test
Loading temperature derivative of stress	$\left(\frac{\partial\sigma}{\partial T}\right)_L$	MPa/°C	0	MDT
Loading start of transformation stress	σ_L^S	MPa	483	Test
Loading end of transformation stress	σ_L^E	MPa	610	Test
Reference temperature	T_0	MPa	37	-
Unloading temperature derivative of stress	$\left(\frac{\partial\sigma}{\partial T}\right)_U$	MPa/°C	0	MDT
Unloading start of transformation stress	σ_U^S	MPa	388	Test
Unloading end of transformation stress	σ_U^E	MPa	256	Test
Loading start of transformation stress (compression)	σ_{CL}^S	MPa	610	Test
Volumetric transformation strain	ε_V^L	-	0.04	Test
Number of annealings to be performed during analysis	N_A	-	0	-

Table 2. Radial compliance (C_D) for physiological diastolic-systolic blood pressure range 80-120 mmHg and maximum values of maximum principal stress (σ_{\max}) and maximum principal strain (ϵ_{\max}) at 120 mmHg for each mesh model. The mesh design is notated by EL for even loop geometry and UL for uneven loop geometry and the wire thickness in mm given in parentheses. Exact analysis pressure values $\Delta P(C_D)$ and $P(\sigma_{\max}, \epsilon_{\max})$ for compliance and stress/strain are given as they varied for numerical reasons.

	Model					
	EL(0.05)	EL(0.0635)	EL(0.075)	UL(0.05)	UL(0.0635)	UL(0.075)
C_D [%/100mmHg]	2.51	0.92	0.63	1.17	0.52	0.51
$\Delta P(C_D)$ [mmHg]	80-121	80-123	79-120	80-123	78-117	74-115
σ_{\max} [MPa]	268	132	91	175	84	80
ϵ_{\max} [%]	0.7	0.43	0.39	0.71	0.41	0.32
$P(\sigma_{\max}, \epsilon_{\max})$ [mmHg]	121	123	120	123	117	115

Figures

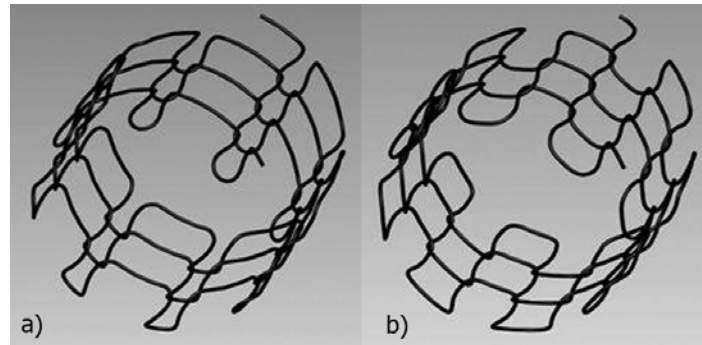


Figure 1. Three-dimensional CAD geometry of the knitted mesh structure with internal diameter of 3.3 mm and Nitinol wire thickness of 0.0635 mm. a) Uneven loop geometry featuring pairs of alternating narrow and wide loops in circumferential direction. b) Even loop geometry with all loops having equal width.

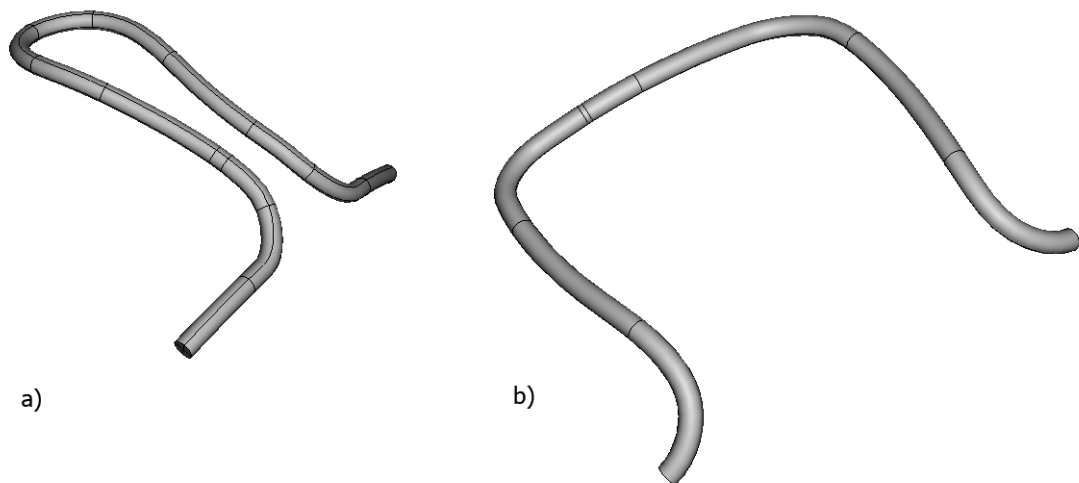


Figure 2. Three-dimensional CAD geometry of a single loop representing a 45° circumferential section of the mesh (wire thickness: 0.0635 mm). This repeating geometrical unit was used to create the partial mesh assembly used in the numerical model. a) Narrow loop of the uneven loop geometry. Boundaries of longitudinal and circumferential partitions are visible as solid dark lines. A respective 45° single loop geometry was used for other wire thicknesses and the even loop geometry. b) Wide loop used for validation of the partial representation of the uneven loop geometry. Only longitudinal partition boundaries are visible.

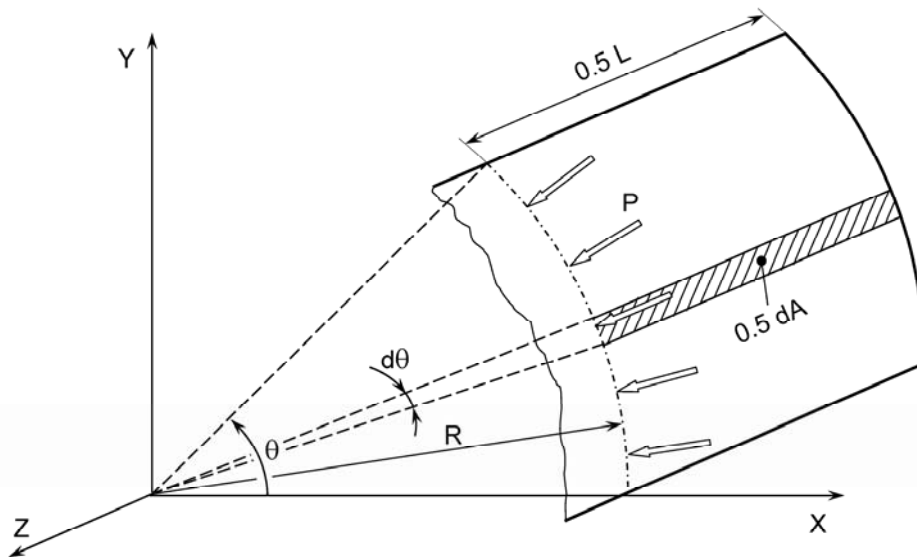


Figure 3. Schematic illustrating the cylindrical expander surface with radius R , length L and subtending angle θ in the mesh co-ordinate system (Z : longitudinal mesh axis, X, Y : radial directions). The radius, length, and subtending angle of the expander coincide with initial internal radius, length, and circumferential section (45°) of the loop assembly. P denotes the uniform pressure over the entire expander surface equivalent to the reaction force of the loop assembly onto the expander upon expander dilation. The angular increment $d\theta$ and the surface area increment dA were used in the integration algorithm to calculate pressure P . (Note that only one longitudinal half-section of the expander surface is shown.)

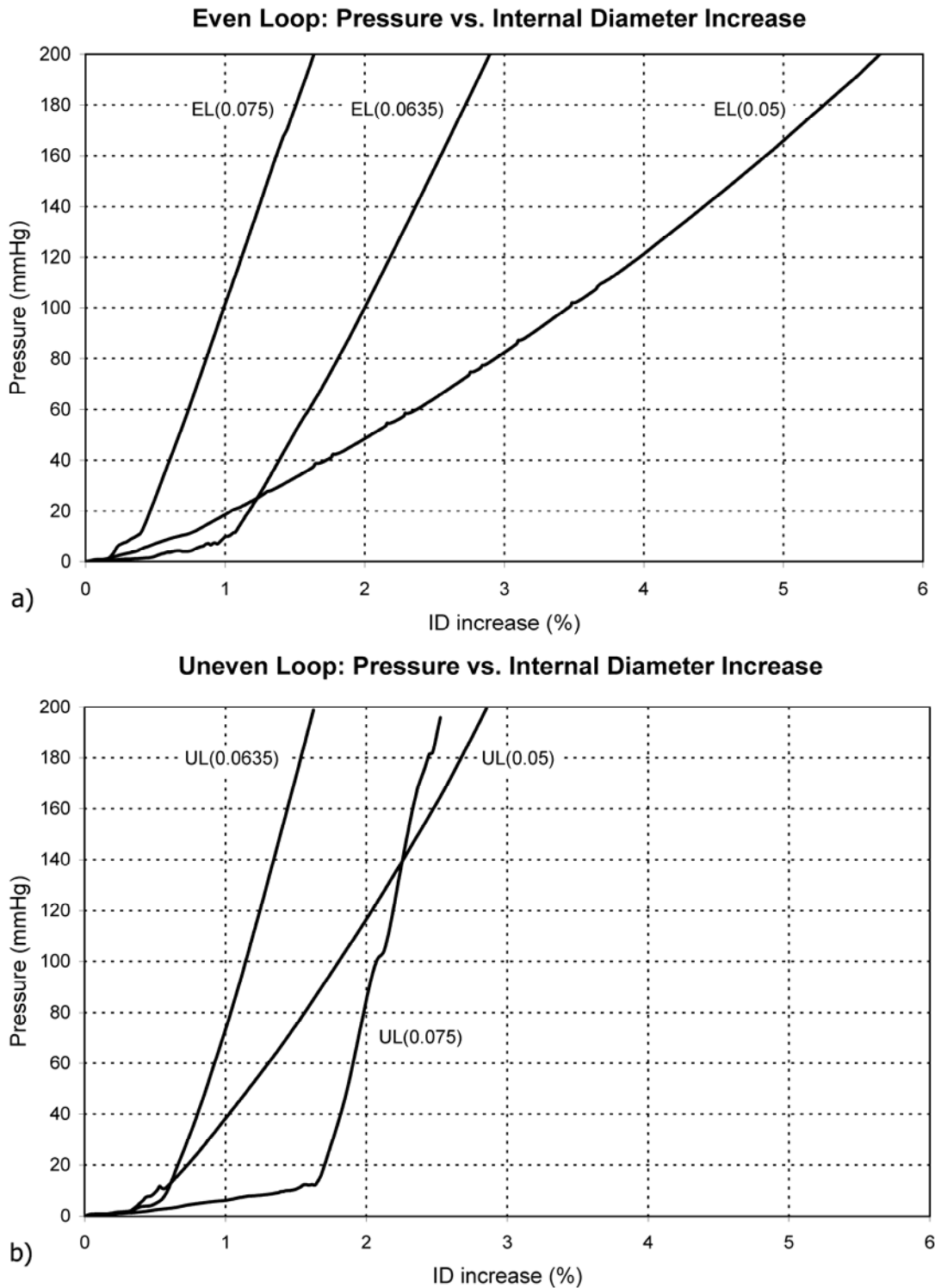


Figure 4. Graphs of equivalent pressure on the expander surface versus increase in internal diameter of the mesh upon radial expansion of the expander for Nitinol wire thicknesses of 0.05 mm, 0.0635 mm, and 0.075 mm. a) Even loop geometry. Different models are referred to by EL(wire thickness). b) Uneven loop geometry. Different models are referred to by UL(wire thickness).

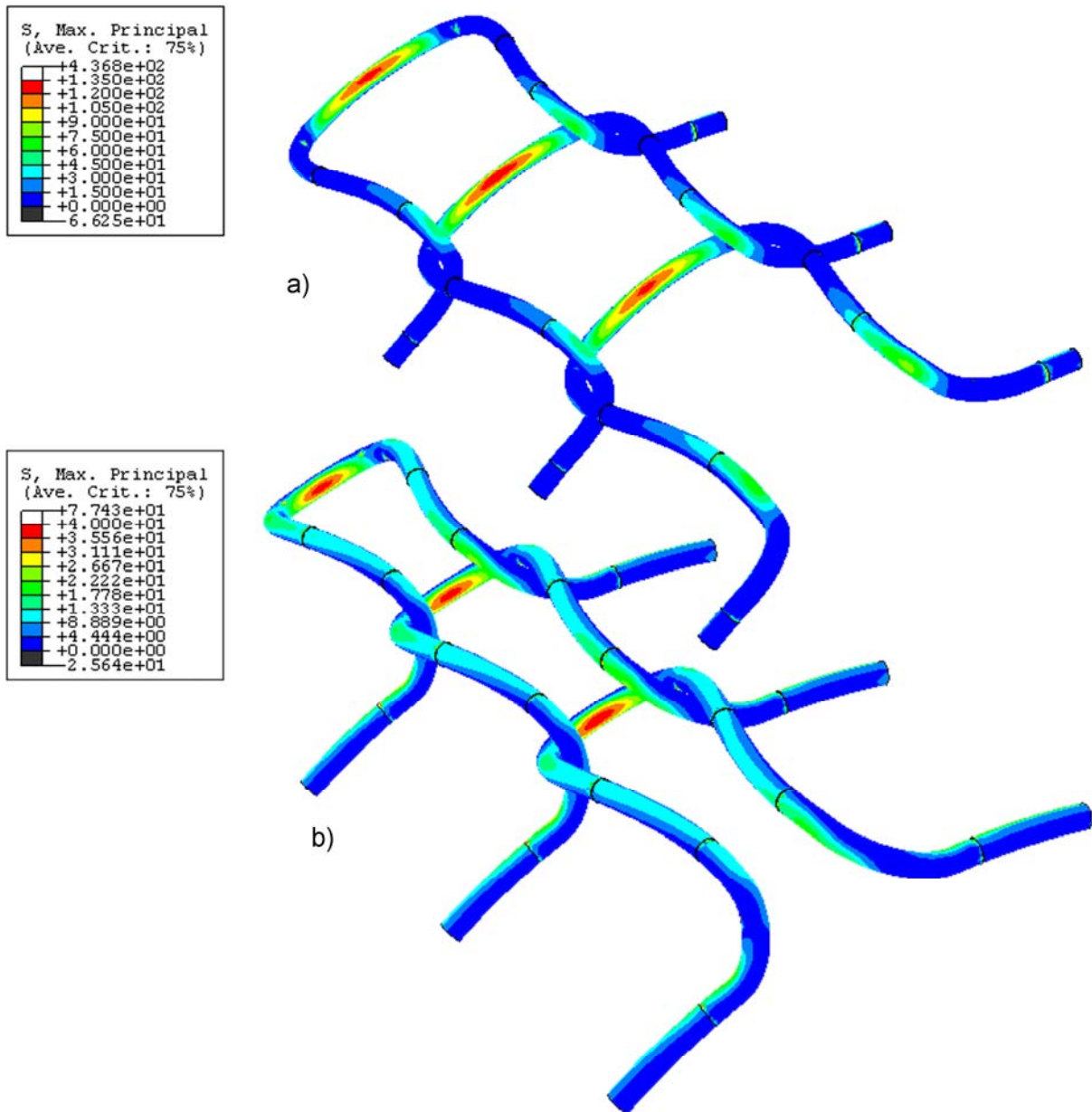


Figure 5. Contour plot of maximum principal stress in loop assembly with 0.0635 mm wire thickness for a) even loop geometry and b) uneven loop geometry. The stress distribution is representative for models with wire thickness of 0.05 mm and 0.075 mm. Note that partial loops on longitudinal ends of loops assembly used for boundary conditions have been removed for display purposes. (The colour version of this figure is available as web site supplement material.)

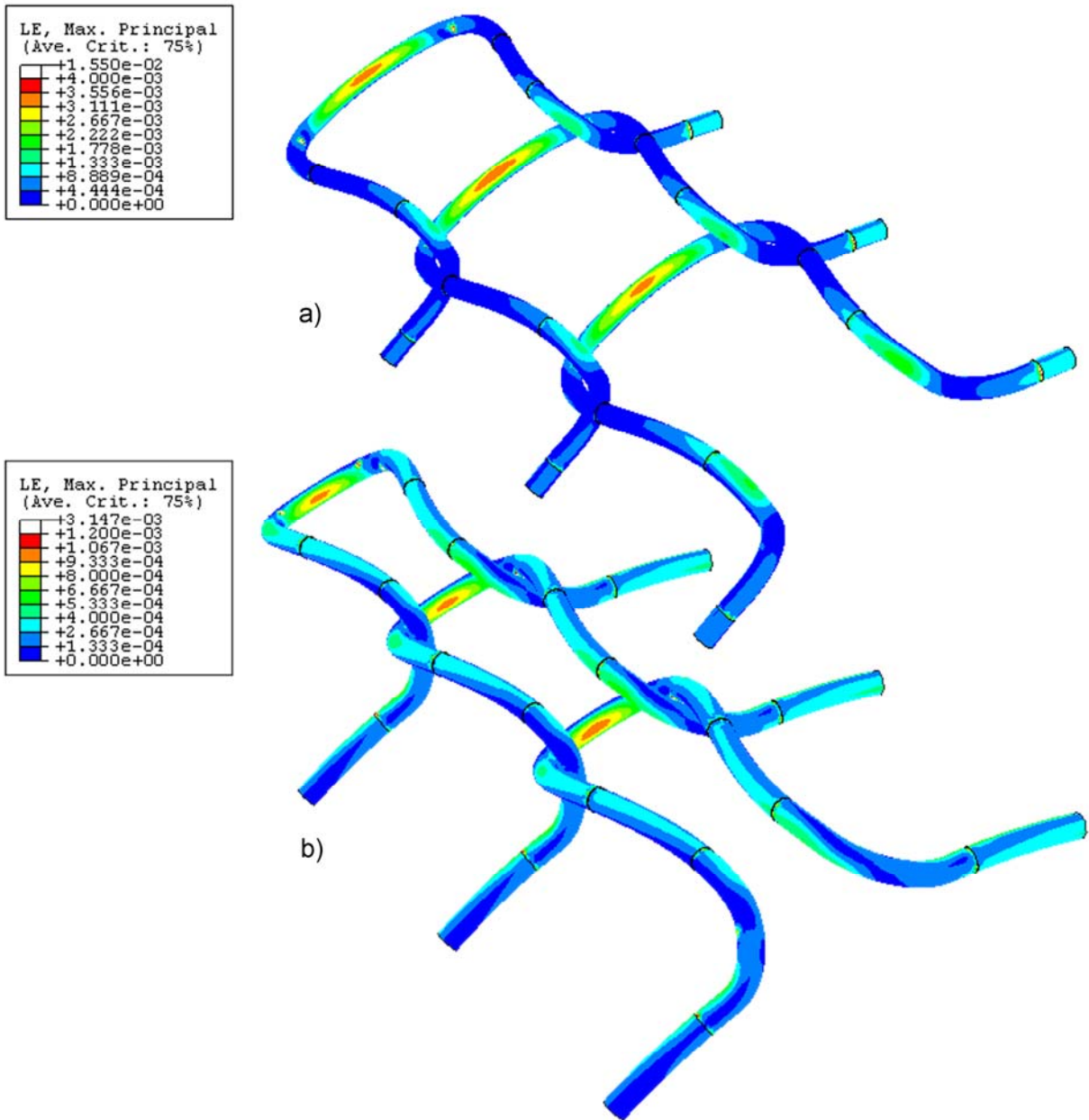


Figure 6. Contour plot of maximum principal strain in loop assembly with 0.0635 mm wire thickness for a) even loop geometry and b) uneven loop geometry. The strain distribution is representative for models with wire thickness of 0.05 mm and 0.075 mm. Note that partial loops on longitudinal ends of loops assembly used for boundary conditions have been removed for display purposes. (The colour version of this figure is available as web site supplement material.)